Synthesis and Properties of Nanostructured Tungsten Oxide on Au(111)

Rishav Harsh, Mariem Ben Youssef, Cyril Chacon, Vincent Repain, Amandine Bellec, Yann Girard, Sylvie Rousset, Jean-Yves Piquemal, Mahamadou Seydou, Philippe Decorse, et al.

Synthesis and Properties of Nanostructured Tungsten Oxide on Au(111)

Rishav Harsh,[†] Mariem Ben Youssef,[‡] Cyril Chacon,[†] Vincent Repain,[†] Amandine Bellec,[†] Yann Girard,[†] Sylvie Rousset,[†] Jean-Yves Piquemal,[‡] Mahamadou Seydou,[‡] Philippe Decorse,[‡] Philippe Lang,[*,‡] and Jérôme Lagoute[*,†]

†*Université de Paris, Laboratoire Matériaux et Phénomènes Quantiques, CNRS, F-75013, Paris, France*

‡*Universit de Paris, ITODYS, CNRS, UMR 7086, 15 rue Jean-Antoine de Baïf, 75205 Paris Cedex 13, France.*

E-mail: lang@univ-paris-diderot.fr; jerome.lagoute@univ-paris-diderot.fr

Abstract

WO_3 nanostructures have been synthesized on Au(111) through solution processing. Three types of structures have been obtained, reticulated polymeric structures, two dimensional WO_3(111) and three-dimensional islands. Their electronic properties have been probed by scanning tunneling spectroscopy. The reticulated structure has a featureless spectrum . WO_3(111) shows n-type semiconducting properties with resonances corresponding to surface states arising from W *5d* states. Those oxyde nanostructures are efficiently decoupling the electronic states of molecular adsorbates from the metal substrate.

Introduction

Tungsten oxides (WO_x, $2 < x < 3$) are extensively studied functional materials with a broad range of applications spanning from electrochromic devices[1] to solar cells,[2] optoelectronics,[3] catalysis[4] and gas sensing.[5,6] WO_3 thin films have been produced and studied using Scanning tunneling microscopy (STM).[7–10] Besides WO_3 and its hydrated forms (also known as tungstic acids), there is a very rich family of non-stoichiometric WO_x oxides. As regards WO_3 specifically, several polymorphs exist depending on the way WO_6 octaedra are interconnected. The monoclinic I (γ-WO_3) polymorph is recognized as the most common and stable phase at room temperature. WO_3 is a n-type wide bandgap semiconductor but possesses an efficient hole transport property due to its high workfunction,[11] that is exploited in photovoltaic devices.[12] The conduction band of WO_x is dominated by the W *5d* states and the valence band is dominated by the O *2p* states.[13,14] Compared to bulk materials, different effects can be expected when tungsten oxides are nanostructured:[15] i) increased surface-to-volume ratios, hence higher specific surface areas, ii) significantly altered surface energies and iii) quantum confinement effects that lead to significant modifications of charge transport, electronic band structure and optical properties. As regards this last point, optical absorption is modified in films made of WO_3 nanowires,[16] while in nanocrystalline

films the electrical bandgap increases with size reduction due to quantum confinement effect.[17] From a structural point of view, several effects have also been reported. For instance, the temperature of phase transitions is lowered in WO_3 nanoparticles,[18] or the formation of a non-expected polymorph: WO_3 nanoplatelets prepared by electrochemical anodization crystallize mainly in the orthorhombic system instead of the expected monoclinic phase.[19] Mastering the synthesis of tungsten oxide nanostructures and the link between structure and physical properties is a forefront challenge for improving WO_x based devices and opening new opportunities in the exploitation of this material. Several synthetic methods have been developed to access well-controlled WO_3 nanostructures. They can be classified in two main groups: solid-phase and liquid-phase syntheses, the latter being generally used for the elaboration of 2D WO_x nanostructures.[20] For liquid-phase syntheses, sol-gel methods have been widely implemented.[15] Precursors such as chlorides or alkoxides can be used, but their high reactivity towards water can lead to uncontrolled condensation reactions.[21] Tungsten peroxo species are thus generally preferred. They are prepared very easily by reacting W metal or even the oxide with hydrogen peroxide, leading to the formation of low-nuclearity peroxo metal complexes.[22] In these compounds the bidentate chelating peroxo ligand (O_2^{2-}) decreases the functionality of aqueous precursors towards condensation and prevents precipitation. Here we have synthesized WO_3 nanostructures by liquid phase synthesis, using tungsten peroxo species, that have been deposited on a Au(111) substrate and thermally treated subsequently. Scanning tunneling microscopy and spectroscopy reveals the formation of three types of nanostructures with different electronic properties: i) reticulated structure with a featureless spectrum, ii) WO_3(111) two dimensional structures revealing n-type semiconducting properties and the formation of a surface state and iii) three-dimensional islands.

Methods

WO_3 powder (1.25 g, 5 mmol) was first added to a 30% solution of aqueous hydrogen peroxide (4 mL, 35 mmol). After 1 h stirring at 60°C, the colorless suspension was cooled at room temperature and centrifuged (15 min at 2000 rpm) to remove the unreacted solid. The resulting supernatant solution, containing the tungsten(VI) peroxo complexes, is stored in a refrigerator and used within a few hours. Just before use, a diluted solution of the precursor (1:1000 vol:vol) is prepared in isopropanol.

Substrates made of a 200 nm thick gold layer sputtered on mica sheets have been used (Phasis). They were cleaned by immersion in a 1/1 ultrapure water/ethanol mixture for 2 min and blown dry under an argon flow. The samples were flamed with a hydrogen blowtorch. After this process, the surface exhibits large (111) oriented atomic terraces (typical width 100 nm). The immersion of the substrates in the precursor solution takes place just after the gold flaming. Thin WO_3 films are prepared by drop casting of isopropanol solution on the gold substrate followed after the drying by an annealing at 450-500°C for 60 mn. The global reaction of WO_3 oxide film formation is written:

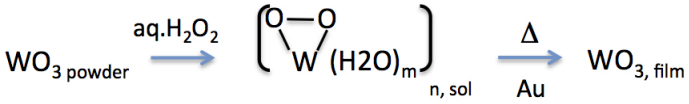

X-ray photoelectron spectroscopy (XPS) signals were recorded using a Thermo VG ESCALAB 250 system equipped with a monochromatic Al $K\alpha X-raysource(1486.6eV)and400\mu$m sized X-ray beam, with a magnetic lens, which increases the electron acceptance angle and hence the sensitivity. The spectra were acquired in the constant analyzer energy mode, with a pass energy of 100 and 40 eV for the survey and the narrow regions, respectively. The peak binding energy positions were calibrated by setting the Au(4f) component at 84 eV .

Density functional theory (DFT) calculations were carried out with a plane-wave basis set by using the Vienna Ab Initio Simulation Package (VASP).[23] In this case, the projector augmented-wave method (PAW) were used to describe the electron-ion interactions.[24,25] The Kohn-Sham equations are solved by means of the Perdew-Burke-Ernzerhof (PBE) func-

tional.[26] We used a convergence value of 500 eV for the cut-off energy. The k-points grid was set to (6×6×6) for the bulk cell optimization and (9×9×9) for accurate density of states calculations. The energy convergence was achieved at 10^{-4} eV/cell and 10^{-6} eV/cell for geometry optimization and density of states calculations, respectively.

The monoclinic-γ tungsten trioxide (WO_3) bulk structure is used from crystal database.[27,28] Using the above method, we realized a full optimization of both lattices parameters and atomic positions. The optimized bulk cell parameter is (a = 7.566 Å, b= 7.655 Å, c= 7.791 Å and α=90°, β=89.7°, γ=90°, in good agreement with the experimental with a deviation lesser than 3.5%[27] and other theoretical works.[29,30] The interatomic d_{W-O} distances is found to vary between 1.786 to 2.136 Å and d_{W-W} vary between 3.822 and 3.857 Å. The optimized unit cell parameters are found to 10.5 Åand 10.7 Å.

The WO_3 (111) surface was represented using the model of a slab composed of six W atomic layers along the z axis (2 W atoms by layer) and a vacuum height of 25 Å. We built the ($2\sqrt{3}\times2\sqrt{3}$) R30 Au(111) superstructure is built from the Au(111) unit cell surface previously optimized. The lattice constant of this superstructure is worth 10.23 . We then deposited the oxide on this surface by relaxing both the atomic positions (of the two upper layers of gold and all of the layers of WO_3) and lattice parameters. The new supercell parameters are found to 10.29 Åand 10.31 Å. For the surface, the k-points grid was set to (3×3×1) for geometry optimization and (9×9×1) for accurate density of states calculations. STM simulation images are obtained by the integrated LDOS calculations within Tersoff-Hamann Theory.[31]

During geometry optimization, the surface, the two upper layers are fully relaxed. The interatomic d_{W-O} and d_{W-W} distances are reduced relative to the bulk.

The minimum d_{W-O} achieves 1.75 Å, slightly lesser than the minimum value in the bulk. The minimum distance d_{W-W} achieves 3.54 Å in the upper layer while it approaches the bulk value in the bottom layers. At the interface, a significant displacements out of the plane of some Au (111) top layer atoms with vertical spacing achieving 0.5 Å. The Au-W bonds were

setting with a bond length of 2.70 Ålesser than Au-Au bond lengths (2.83 Åin the bulk).

STM measurements were performed with a low-temperature STM apparatus (Omicron) working at 4.6 K at a pressure lower than 1×10^{-10} mbar. Note that the sample was prepared in air before being transfered to the vacuum system, which means that the oxide structures observed are stable in air. The dI/dV spectra were acquired using a lock-in detector at a frequency of ca. 823 Hz and a modulation amplitude of 35 mV. The measurements were performed with an electrochemically etched tungsten tip.

Results and Discussion

The solution based synthesis process used here leads ot the formation of WO_3 as evidenced by XPS spectra measured on a thin film grown on Au(111) (see Figure 1a) and infrared spectroscopy and X-ray diffraction (see supporting information). Figure 1a exhibits the XPS spectra of an oxide film on gold. The oxide thickness is globally estimated to 0.8 $\pm$ 0.2 nm via the attenuation of the gold signal by the WO_3. The binding energies of the main components W $4f_{7/2}$ and W $4f_{5/2}$ lines have been found at 35.86 eV and and 38.00 eV, corresponding to W(VI) (referenced to Au 4f at 84 eV).[32] More precisely the deconvolution of the spectrum leads to two small supplementary components corresponding to W(V); the ratio of the intensities of 7/2 on 5/2 components agrees with the expected ratio for both W(V) and W(VI). We find at least 90% of W(VI) or WO_3 (see table in SI) . The O 1s spectrum is thin and located at 530.62 (FWHM 1.47eV) in agreement with the main feature of WO_3. All these observations account for the formation of WO_{3-x} with $x < 0.1$. After the synthesis of a submonolayer of WO_3, the sample surface is covered in majority by reticulated polymeric strucures (structure S1) shown in Figure 1b with a height of 2 Å. Oxide islands (denoted S3) are also present on the surface with a typical height of 1.2 nm and lateral size in the 10 to 30 nm range. The S3 structures exhibit a rough surfaces with around 1 Å height variation and the presence of clusters with heights between 5 and 10 Å and width

of about 5 Å. The roughness of these structures suggests that defects can be present which may contain eventually W(V) atoms as detected by XPS. Another morphology of oxide that forms on the surface is shown in Figure 1c consisting in periodic bidimensional structure (denoted S2). The height with respect to the Au(111) substrate is of 0.7 nm. The height of the 3 structures indicates that the number of oxide layers increases from S1 to S2 and S3 structures and is limited to a few number of layers (see supporting information). The Fourier transform of the STM image of the S2 structure allows to determine a periodicity of 0.95 ± 0.05 nm. This periodicity corresponds to an epitaxial relation with the oxide forming a $(2\sqrt{3}\times 2\sqrt{3})$ R30 pattern (see supporting information). This structure is unexpected since it has not been reported before. The growth of tungsten oxide on Pt(111) has been shown to lead to a 3×3 pattern,[33,34] giving a periodicity of about 8.0 ± 0.3 Å measured by STM. This structure is made of an array of molecularly bound $(WO_3)_3$ leading to a honeycomb-like pattern in the STM images. Our case is different since the period is larger and we observe a hexagonal pattern of bright lobes instead of the holes observed on Pt(111). For a WO_3 thin film on $LaAlO_3$(100), the WO_3 surface orientation was reported to be (100) with a square or rectangular pattern at the surface depending on surface reconstruction.[35] Moreover, the S2 pattern that we observe is not expected by considering trivial low index surfaces from the ideal cubic structure.[15] For unreconstructed low index surfaces, a square pattern is expected for the (100) surface, a rectangular pattern for the (110) surface and a hexagonal pattern is expected for the (111) surface but with a periodicity of about 5 Åthat is close to half of the observed one. However, considering the (111) surface, an unreconstructed stoichiometric surface is polar and corresponds to a type 3 surface according to the Tasker classification.[36] To remove the surface dipole and charge, non-stoichiometric reconstructed surface can be formed[37] where half of surface atoms are removed leading to a 2×2 pattern. Such surface reorganization explains well the S2 structure that we observed as confirmed by our ab initio calculations.

In Figure 2a we show the (111) surface plane of the monoclinic phase of WO_3 on Au(111)

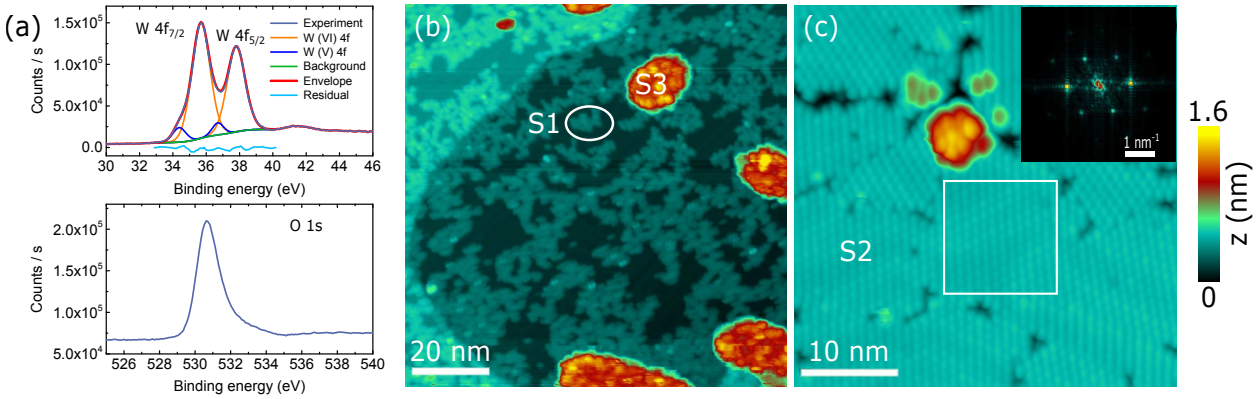

Figure 1: (a) XPS spectra of a WO_3 thin film on Au(111). (Top) Deconvoluted spectrum at the W 4f threshold. (Bottom) Spectrum at the O 1s threshold. (b) STM image of WO_3 nanostructures on Au(111) (1.5 V, 10 pA). Two types of nanostructures noted S1 and S3 are observed. (c) Typical bidimensional structure (S2) observed on the sample (1.5 V, 20 pA). The black dotted lines indicate ridges of the Au(111) surface reconstruction that can be seen through the S2 structure. The inset shows the FFT of the area enclosed within the white box. The scale bar on the right applies to the two STM images in (b) and (c).

with the 2×2 pattern, where half of the W surface atoms are removed, as described above which account for the experimental STM images. We used a 6 layers WO_3 slab deposited with its plane (111) on a 4 layers Au(111) forming a $2\sqrt{3}\times2\sqrt{3}$ R30 layer corresponding to the epitaxial relation obtained experimentally (more details in the supporting information). The W atoms belonging to the top atomic layer form a hexagonal pattern as can be seen from the top view. The unit cell vectors have a length of 1.03 nm. We have calculated the corresponding STM image obtained by a contour plot of integrated isodensity (Fig. 2b). As can be seen, the calculated image shows a hexagonal pattern with bright lobes corresponding to the W atoms of the top layer. This image is calculated at +1.5 V and therefore integrate the conduction band of WO_3 that derives from the W *5d* states,[13,14] which explains that the STM image is dominated by the orbitals of the W atoms. The experimental STM image of the 2D structure reported in Figure 2c shows the hexagonal pattern of the S2 structure that compares well also with the calculated image. The linescan of Figure 2d shows the periodicity of 1 nm in this structure that corresponds to the periodicity observed in the calculated image. Therefore, we attribute the nanostructure S2 to a bidimensional WO_3 cristal with a non-stoichiometric monoclinic (111) surface. Note that the experimental

image present an elongated shape as compared to the calculation that is attributed to a tip effect. In order to investigate the electronic properties of the 3 nanostructures we performed scanning tunneling spectroscopy measurements on an area where all structures are observed, allowing for reliable comparison of data measured with the same tip state on the same area.

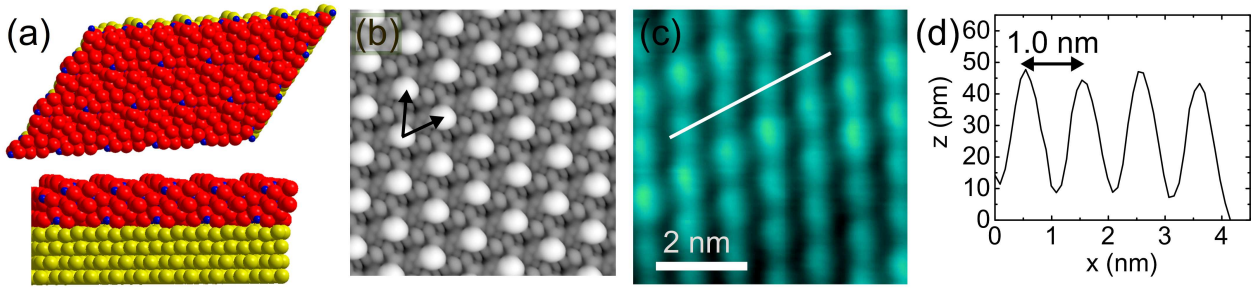

Figure 2: (a) Side view (bottom) and top view (top) of the structure of a (111) surface of a WO_3 slab on Au(111). Color code: blue for tungsten, red for oxygen, yellow for gold. (b) Simulated STM image of a WO_3(111) surface at 1.5 V. The arrows indicate the surface unit cell vectors. (c) STM image (zoom of Figure 1c) of the bidimensional tungsten oxide structure. (d) Linescan corresponding to the line displayed in (c).

The STM topography shown in Figure 3a reveals the structures S1, S2 and S3 coexisting on the same sample location. The electronic properties of all structures are revealed by $I(V)$ and dI/dV curves shown in Figure 3b,c. The reference spectrum measured on the Au(111) surface reveals the expected metallic behaviour in I(V) and dI/dV signals with a step around -0.5 V corresponding to the Shockley state.[38] The spectroscopy of the S1 structure shows characteristics which are similar to the Au(111) substrate. We attribute this feature to the fact that the oxide in this phase behave as a semiconductor with a wide bandgap through which the spectroscopy of Au(111) is measured. Therefore the spectroscopy of the S1 structure is featureless and is dominated by the Au(111) density of states. The S2 and S3 oxides are markedly different with a rectifying characteristic as seen in their (I-V) curves. The WO_3(111) shows two peaks in the local density of stets (LDOS) at +0.7 V and +1.3 V followed by an exponential increase at 1.6 V with respect to the Fermi level (zero sample bias voltage). The S3 structure shows an exponential increase in the LDOS with an onset at 0.85 V determined from the log(dI/dV) curve (inset of Figure 3c). The exponential

onsets are attributed to the conduction band minimum (CBM) of the WO_3 nanostructures. The valence band maximum (VBM) is lower than -2 V with respect to the Fermi level. In order to interpret these values it is worth to compare with experimental determinations of the electronic bands of WO_3 in thin films.[39] The CBM and VBM were determined to be at 0.39 eV and -2.89 eV respectively with respect to the Fermi level positioned at 4.49 eV from the vacuum level. The contact potential (difference of work functions) of Au(111) and WO_3 may shift the WO_3 states upwards by 0.8 eV. Considering that the thickness of the WO_3 nanostructures on Au(111) is small with respect to the extent of the charge space region, this would give a CBM at 1.2 V and a VBM at -2.08 V. Obviously the nanostructuration and interaction with the Au(111) substrate is expected to modify the electronic structure of the oxide. It was reported that the size reduction increases the bandgap.[17] Therefore the position of a CBM around 1.2 eV and a VBM far below the Fermi level is expected for a WO_3 nanostructure on gold. These considerations explain the rectifying behaviour observed experimentally on the S2 and S3 structures, and also the variation of electronic properties of WO_3 with a CBM of 1.6 V for S2 and 0.85 V for S3 and a gap above 3.6 V for S2 that is larger than the reported bulk values (with a VBM below -2 V for S2 and S3).

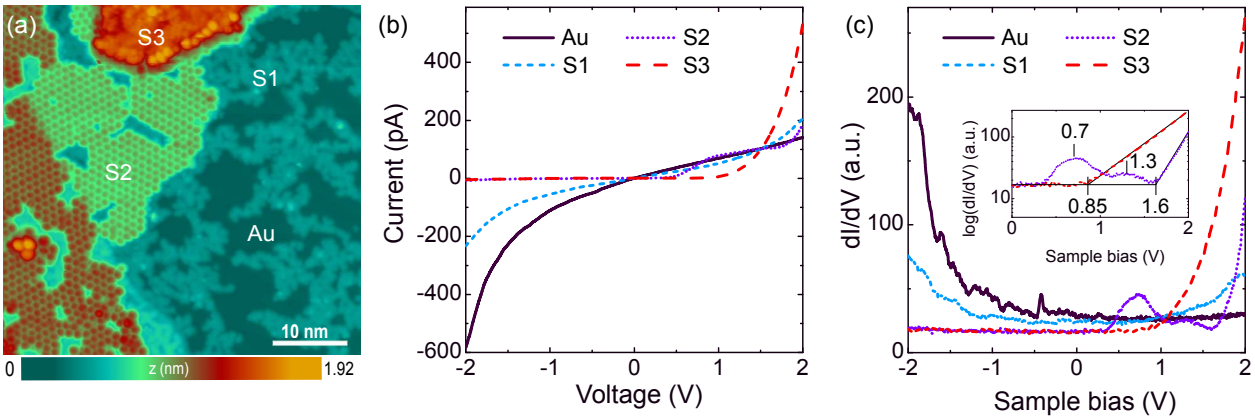

Figure 3: (a) STM image of an area of WO_3 on Au(111) where 3 types of nanostructures appear (1.5 V, 10 pA). (b) I(V) spectra measured above each type of nanostructure and reference spectrum on Au(111). (c) dI/dV spectra corresponding to the I(V) curves shown in (b).

In the S2 structure the two peaks below the CBM are attributed to surface states. Indeed,

at the surface of WO_3 since half of the W atoms are present, the W surface atoms are quite isolated as compared to the bulk ones, and therefore it is expected that they exhibit quasi atomic resonant states. This interpretation is supported by our ab initio calculations. We have performed PDOS calculations for the WO_3 slab on Au(111) previously described. The PDOS has been calculated for the *sp* states of oxygen atoms in the bulk (atoms in the middle of the slab) and *d* states of W atoms in the bulk and at the surface. The calculations show a band gap delimited by *sp* states of O atoms at -2.5 eV for the VB, and *d* states of W at 1.1 eV for the CB (Figure 4). The calculated VB and CB edges agree well with the experiment that gives a CBM at 1.6 V and a VBM below -2 V. The discrepancy between the calculated and experimental VBM is attributed to the usual underestimation of electronic gap in DFT calculations. The PDOS of W surface atoms shows peaks at positive voltage inside this gap, which supports the interpretation that the peaks observed on the S2 structure are surface states of WO_3(111) arising from the *d* states of surface W atoms. For the three types of WO_3 structures, we have observed semiconducting properties. Among all possible interests of these nanostructures, we have tested their potential for molecular electronics.

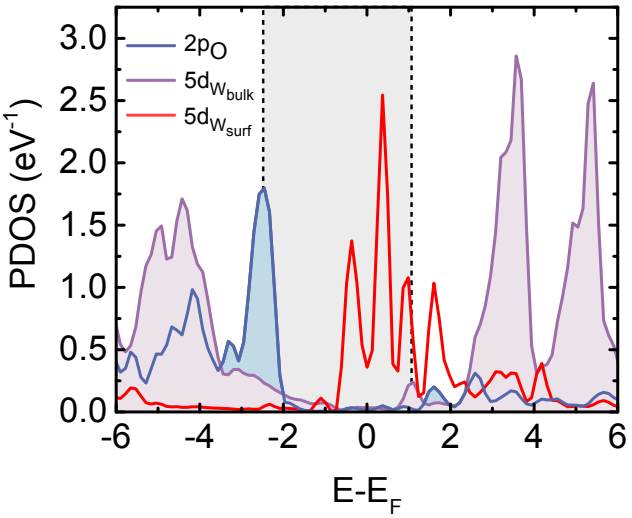

Figure 4: Calculated PDOS of WO_3(111) on Au(111) for bulk O and W atoms and surface W atom. The gray area indicates the gap defined by bulk atoms of the WO_3 slab.

Non metallic thin films on metals can be used as decoupling layers for adsorbates allowing to access to intrinsic properties of molecules adsorbed on these surfaces.[40] In order to probe

the potential use of WO_3 as a decoupling layer, we have deposited free base tetraphenylporphyrin (H_2TPP) molecules on our sample. These molecules have been previously studied on Au(111)[41] and the effect of the interaction with a surface has been discussed by comparing Au(111) and graphene substrates.[42] Here we show how WO_3 nanostructures affect the molecule-surface interaction.

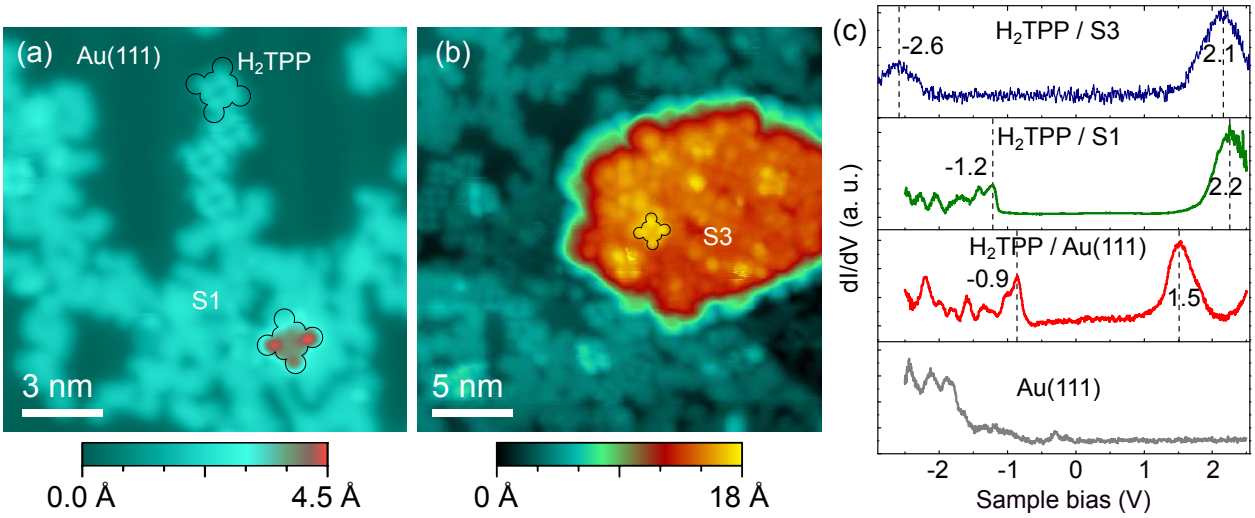

Figure 5: (a) STM image of H_2TPP molecules adsorbed on WO_3 on Au(111) in an area with 1D nanostructures (1.5 V, 100 pA). (b) Same as (a) in another area where 1D and 3D nanostructures are present (2.4 V, 100 pA). (c) From bottom to top, dI/dV spectra of Au(111), H_2TPP on Au(111), H_2TPP on 1D nanostructures and H_2TPP on 3D nanostructures measured in the area shown in (b).

After H_2TPP deposition, the sample was annealed to room temperature in order to allow for the diffusion and stabilization of the molecules. After that procedure, the molecules were not observed on the S2 structure, which may indicate a lower diffusion barrier on S2. In Figure 5 we show a sample area with a WO_3 structure S1 on which H_2TPP molecules have been deposited. The dI/dV spectroscopy of H_2TPP adsorbed on the S1 structure shows resonant states with peaks corresponding to the frontier orbitals at -1.2 V and 2.2 V, corresponding to the HOMO and LUMO states respectively, leading to an electronic gap of 3.4 V (Figure 5c). This gap is larger than the gap of 2.4 V measured on H_2TPP on Au(111) in agreement with our previous reports.[41] This increase of gap is expected when a molecule is decoupled from the metallic substrate by an insulating layer, due to a reduced screening

effect.[43] The larger gap measured on H_2TPP on S1 confirms the non metallic character of S1 described above. Moreover, this gap is lower than the expected intrinsic gap of H_2TPP of 4.7 V[42,44] due to a partial reduction of the screening effect. In Figure 5b we show H_2TPP molecules adsorbed on a S3 structure that is thicker than S1. The molecular spectrum of H_2TPP in that case is of 4.7 V and agrees with the gap of a molecule in its gaz phase. Therefore, a stronger decoupling effect is observed for the S3 structure.

Conclusions

In conclusion, WO_3 nanostructures have been synthesized at the surface of Au(111). The solution process leads to 3 types of structures. Reticulated polymeric strucures with featureless electronic spectrum. Two dimensional WO_3(111) exhibiting n-type semiconducting electronic properties with 2 resonant states below the VBM corresponding to surface states of WO_3(111). Islands of WO_3(111) are the third type of nanostructures with a CBM at a lower energy than the 2D structure attributed to the fact that the gap is increased in the 2D structure due to electronic confinement. Finally, WO_3 are shown to be efficient decoupling layers for molecular adsorbates. These findings reveal the variety of structural and electronic properties achievable with WO_3 nanostructures opening exciting perspectives for applications based on this material.

Supporting Information Available

Infra red spectroscopy, X-ray diffraction of WO_3, Height of oxide nanostructures, Orientation of the S2 nanostructure, Optimized geometry of WO_3 on Au(111).

Acknowledgement

We thank the Indo-French Centre for the Promotion of Advanced Research (CEFIPRA) for financial support. We thank Andrés Lombana for stimulating discussions and Sophie Nowak for XRD measurements.

References

(1) Buch, V. R.; Chawla, A. K.; Rawal, S. K. Review on electrochromic property for WO_3 thin films using different deposition techniques. *Mater. Today:. Proc.* **2016**, *3*, 1429–1437.

(2) Zheng, H.; Tachibana, Y.; Kalantar-Zadeh, K. Dye-sensitized solar cells based on WO_3. *Langmuir* **2010**, *26*, 19148–19152.

(3) Hai, Z.; Wei, Z.; Xue, C.; Xu, H.; Verpoort, F. Nanostructured tungsten oxide thin film devices: from optoelectronics and ionics to iontronics. *J. Mater. Chem. C* **2019**, *7*, 12968–12990.

(4) Wang, Y.; Tian, W.; Chen, C.; Xu, W.; Li, L. Tungsten trioxide nanostructures for photoelectrochemical water splitting: material engineering and charge carrier dynamic manipulation. *Adv. Funct. Mater.* **2019**, *29*, 1809036.

(5) Stankova, M.; Vilanova, X.; Llobet, E.; Calderer, J.; Bittencourt, C.; Pireaux, J.-J.; Correig, X. Influence of the annealing and operating temperatures on the gas-sensing properties of rf sputtered WO_3 thin-film sensors. *Sens. Actuators, B* **2005**, *105*, 271–277.

(6) Dong, C.; Zhao, R.; Yao, L.; Ran, Y.; Zhang, X.; Wang, Y. A review on WO3 based gas sensors: Morphology control and enhanced sensing properties. *J. Alloys Compd.* **2020**, *820*, 153194.

(7) Santucci, S.; Cantalini, C.; Crivellari, M.; Lozzi, L.; Ottaviano, L.; Passacantando, M. X-ray photoemission spectroscopy and scanning tunneling spectroscopy study on the thermal stability of WO3 thin films. *J. Vac. Sci. Technol.* **2000**, *18*, 1077–1082.

(8) Ottaviano, L.; Bussolotti, F.; Lozzi, L.; Passacantando, M.; La Rosa, S.; Santucci, S. Core level and valence band investigation of WO3 thin films with synchrotron radiation. *Thin Solid Films* **2003**, *436*, 9–16.

(9) Maffeis, T.; Yung, D.; LePennec, L.; Penny, M.; Cobley, R.; Comini, E.; Sberveglieri, G.; Wilks, S. STM and XPS characterisation of vacuum annealed nanocrystalline WO3 films. *Surf. Sci.* **2007**, *601*, 4953–4957.

(10) Bonnell, D. A.; Garra, J. Scanning probe microscopy of oxide surfaces: atomic structure and properties. *Rep. Prog. Phys.* **2008**, *71*, 044501.

(11) Tao, C.; Ruan, S.; Xie, G.; Kong, X.; Shen, L.; Meng, F.; Liu, C.; Zhang, X.; Dong, W.; Chen, W. Role of tungsten oxide in inverted polymer solar cells. *Appl. Phys. Lett.* **2009**, *94*, 043311.

(12) Li, Z. Stable Perovskite Solar Cells Based on WO_3 Nanocrystals as Hole Transport Layer. *Chem. Lett.* **2015**, *44*, 1140–1141.

(13) Bullett, D. W. A theoretical study of the x-dependence of the conduction-band density of states in metallic sodium tungsten bronzes Na_xWO_3. *Solid State Commun.* **1983**, *46*, 575–577.

(14) Hjelm, A.; Granqvist, C. G.; Wills, J. M. Electronic structure and optical properties of WO_3, $LiWO_3$, $NaWO_3$, andHWO_3. *Phys. Rev. B* **1996**, *54*, 2436–2445.

(15) Zheng, H.; Ou, J. Z.; Strano, M. S.; Kaner, R. B.; Mitchell, A.; Kalantar-zadeh, K. Nanostructured tungsten oxide–properties, synthesis, and applications. *Adv. Funct. Mater.* **2011**, *21*, 2175–2196.

(16) Chen, H.; Xu, N.; Deng, S.; Zhou, J.; Li, Z.; Ren, H.; Chen, J.; She, J. Electrochromic properties of WO_3 nanowire films and mechanism responsible for the near infrared absorption. *J. Appl. Phys.* **2007**, *101*, 114303.

(17) Gullapalli, S.; Vemuri, R.; Ramana, C. Structural transformation induced changes in the optical properties of nanocrystalline tungsten oxide thin films. *Appl. Phys. Lett.* **2010**, *96*, 171903.

(18) Boulova, M.; Lucazeau, G. Crystallite nanosize effect on the structural transitions of WO_3 studied by Raman spectroscopy. *J. Solid State Chem.* **2002**, *167*, 425–434.

(19) Sadek, A. Z.; Zheng, H.; Latham, K.; Wlodarski, W.; Kalantar-Zadeh, K. Anodization of Ti thin film deposited on ITO. *Langmuir* **2009**, *25*, 509–514.

(20) Guo, T.; Yao, M.-S.; Lin, Y.-H.; Nan, C.-W. A comprehensive review on synthesis methods for transition-metal oxide nanostructures. *CrystEngComm* **2015**, *17*, 3551–3585.

(21) Livage, J.; Ganguli, D. Sol–gel electrochromic coatings and devices: a review. *Sol. Energy Mater. Sol. Cells* **2001**, *68*, 365–381.

(22) Piquemal, J.-Y.; Briot, E.; Brégeault, J.-M. Preparation of materials in the presence of hydrogen peroxide: from discrete or zero-dimensional objects to bulk materials. *Dalton Trans.* **2013**, *42*, 29–45.

(23) Kresse, G.; Furthmüller, J. Efficiency of ab-initio total energy calculations for metals and semiconductors using a plane-wave basis set. *Comp. Mater. Sci.* **1996**, *6*, 15–50.

(24) Kresse, G.; Joubert, D. From ultrasoft pseudopotentials to the projector augmented-wave method. *Phys. Rev. B* **1999**, *59*, 1758.

(25) Blöchl, P. E.; Jepsen, O.; Andersen, O. K. Improved tetrahedron method for Brillouin-zone integrations. *Phys. Rev. B* **1994**, *49*, 16223.

(26) Perdew, J. P.; Burke, K.; Ernzerhof, M. Generalized gradient approximation made simple. *Phys. Rev. Lett.* **1996**, *77*, 3865.

(27) Chichagov, A. Information-calculating system on crystal structure data of minerals (MINCRYST). Mater. Sci. Forum. 1994; pp 193–198.

(28) Chichagov, A.; Belonozhko, A.; Lopatin, A.; Dokina, T.; Samokhvalova, O.; Ushakovskaya, T.; Shilova, Z. Information computing system from structural data on minerals (Mincryst). *Kristallografiya* **1990**, *35*, 610–616.

(29) Gerosa, M.; Di Valentin, C.; Onida, G.; Bottani, C. E.; Pacchioni, G. Anisotropic effects of oxygen vacancies on electrochromic properties and conductivity of γ-monoclinic WO_3. *J. Phys. Chem. C* **2016**, *120*, 11716–11726.

(30) Tian, F.; Zhao, L.; Xue, X.-Y.; Shen, Y.; Jia, X.; Chen, S.; Wang, Z. DFT study of CO sensing mechanism on hexagonal WO_3 (0 0 1) surface: The role of oxygen vacancy. *Appl. Surf. Sci.* **2014**, *311*, 362–368.

(31) Tersoff, J.; Hamann, D. R. Theory of the scanning tunneling microscope. *Phys. Rev. B* **1985**, *31*, 805–813.

(32) Fleisch, T.; Mains, G. An XPS study of the UV reduction and photochromism of MoO3 and WO3. *J. Chem. Phys.* **1982**, *76*, 780–786.

(33) Li, Z.; Zhang, Z.; Kay, B. D.; Dohnlek, Z. Polymerization of Formaldehyde and Acetaldehyde on Ordered $(WO_3)3$ Films on Pt(111). *J. Phys. Chem. C* **2011**, *115*, 9692–9700.

(34) Li, Z.; Zhang, Z.; Kim, Y. K.; Smith, R. S.; Netzer, F.; Kay, B. D.; Rousseau, R.; Dohnálek, Z. Growth of ordered ultrathin tungsten oxide films on Pt (111). *J. Phys. Chem. C* **2011**, *115*, 5773–5783.

(35) Li, M.; Posadas, A.; Ahn, C. H.; Altman, E. I. Scanning tunneling microscopy study of terminal oxygen structures on WO_3(100) thin films. *Surf. Sci.* **2005**, *579*, 175–187.

(36) Tasker, P. The stability of ionic crystal surfaces. *J. Phys. C: Solid State Phys.* **1979**, *12*, 4977.

(37) Goniakowski, J.; Finocchi, F.; Noguera, C. Polarity of oxide surfaces and nanostructures. *Rep. Prog. Phys.* **2007**, *71*, 016501.

(38) Chen, W.; Madhavan, V.; Jamneala, T.; Crommie, M. Scanning tunneling microscopy observation of an electronic superlattice at the surface of clean gold. *Phys. Rev. Lett.* **1998**, *80*, 1469.

(39) Weinhardt, L.; Blum, M.; Bär, M.; Heske, C.; Cole, B.; Marsen, B.; Miller, E. Electronic surface level positions of WO_3 thin films for photoelectrochemical hydrogen production. *J. Phys. Chem. C* **2008**, *112*, 3078–3082.

(40) Repp, J.; Meyer, G.; Stojković, S. M.; Gourdon, A.; Joachim, C. Molecules on insulating films: scanning-tunneling microscopy imaging of individual molecular orbitals. *Phys. Rev. Lett.* **2005**, *94*, 026803.

(41) Pham, V. D.; Repain, V.; Chacon, C.; Bellec, A.; Girard, Y.; Rousset, S.; Smogunov, A.; Dappe, Y. J.; Lagoute, J. Control of molecule–metal interaction by hydrogen manipulation in an organic molecule. *J. Phys. Chem. Lett.* **2016**, *7*, 1416–1421.

(42) Pham, V. D.; Lagoute, J.; Mouhoub, O.; Joucken, F.; Repain, V.; Chacon, C.; Bellec, A.; Girard, Y.; Rousset, S. Electronic interaction between nitrogen-doped graphene and porphyrin molecules. *ACS Nano* **2014**, *8*, 9403–9409.

(43) Lin, H.; Lagoute, J.; Repain, V.; Chacon, C.; Girard, Y.; Lauret, J.-S.; Ducastelle, F.; Loiseau, A.; Rousset, S. Many-body effects in electronic bandgaps of carbon nanotubes measured by scanning tunnelling spectroscopy. *Nat. Mater.* **2010**, *9*, 235–238.

(44) Blase, X.; Attaccalite, C.; Olevano, V. First-principles GW calculations for fullerenes, porphyrins, phtalocyanine, and other molecules of interest for organic photovoltaic applications. *Phys. Rev. B* **2011**, *83*, 115103.

TOC Graphic